CDF note 9740

An Updated Measurement of the Ratio $\frac{\sigma(B_c^+)*BR(B_c^+ \to J/\psi+\mu^+ +\nu)}{\sigma(B^+)*BR(B^+ \to J/\psi+K^+)}$ Using 1 fb^{-1} of Integrated Luminosity

The CDF Collaboration
URL http://www-cdf.fnal.gov
(Dated: April 15, 2009)

This note describes the B_c^+ production cross section times branching ratio measurement of the decay mode $B_c^+ \to J/\psi+\mu^+ +\nu$ relative to the $B^+ \to J/\psi+K^+$ decay using data with an integrated luminosity of 1 fb^{-1}. We select a sample of 229 (214) events in which a J/ψ candidate is matched with a high quality third muon and the J/ψ decays to two muons for $p_T(B_c^+) > 4$ GeV/c (6 GeV/c). The background contributions from misidentified J/ψ, misidentified muons, and from the different b-hadrons are estimated using data and PYTHIA samples. The total background consists of 111$\pm$8 (107 $\pm$ 8) events. We estimate the ratio of the production cross section times branching ratio of $B_c^+ \to J/\psi + \mu^+ + \nu$ relative to $B^+ \to J/\psi + K^+$ for two $p_T(B_c^+)$ cuts: for $p_T(B_c^+) > 4$ GeV/c as 0.295 ± 0.040 (stat.)$^{+0.033}_{-0.026}$ (syst.) ± 0.036 (p_T spectrum) and for $p_T(B_c^+) > 6$ GeV/c as 0.227 ± 0.033 (stat.)$^{+0.024}_{-0.017}$ (syst.) ± 0.014 (p_T spectrum).

Preliminary Results for Spring 2009 Conferences

I. INTRODUCTION

The B_c^+ meson is the most massive of the bottom-flavored mesons, apart from the $b\bar{b}$ charmonia, with a ground state that consists of a $\bar{b}$ and a c quark [1]. The B_c^+ meson was discovered by CDF in Run I using the $B_c^+ \to J/\psi + \ell^+ + X$ decay modes [2]. The ratio of the B_c^+ production cross section times semileptonic branching ratio in the single muon and electron channels to the production cross section times branching ratio for $B^+ \to J/\psi + K^+$ using an integrated luminosity of 360 pb^{-1} of Run II data was presented in Refs. [3] and [4], respectively. Recently, we measured the B_c^+ lifetime in the $B_c^+ \to J/\psi + \mu^+ + X$ and $B_c^+ \to J/\psi + e^+ + X$ decay channels using an integrated luminosity of 1 fb^{-1} of Run II data [5]. In this note we update the $\frac{\sigma(B_c^+) * BR(B_c^+ \to J/\psi + \mu^+ + \nu)}{\sigma(B^+) * BR(B^+ \to J/\psi + K^+)}$ ratio to an integrated luminosity of 1 fb^{-1}.

II. EVENT SELECTION

The datasets used in this analysis are collected with the J/ψ di-muon trigger and consist of ~ 1 fb^{-1} of integrated luminosity. Our selection requirements closely follow those of the recent B_c^+ semileptonic lifetime measurements [5], in which we search for J/ψ particles reconstructed through the $\mu^+\mu^-$ decay channel that are matched with high quality third muons.

The cuts applied for the $J/\psi \to \mu^+\mu^-$ selection are identical to those used in the B_c^+ semileptonic lifetime analysis [5] and are listed in Table I. The resulting di-muon mass distribution with J/ψ mass peak can be seen in Fig. 1.

Selection Requirement	Value
Two Muons	CMU+CMU or CMU+CMX
Trigger Path Selection	CMUCMU1.5 or CMU1.5_CMX2 Trigger Paths
Muon Likelihood (Bottom Taggers)	> 0.06
CMU Muon p_T	> 1.5 GeV/c
CMX Muon p_T	> 2.0 GeV/c
COT Hits	2 Stereo + 2 Axial Superlayers (5 hits each SL)
Silicon Hits	≥ 3 hits in ϕ layers (SVX+ISL)
J/ψ Mass	$\lvert M_{J/\psi} - 3.09687$ GeV/$c^2\rvert < 0.05$ GeV/c^2

TABLE I: Cuts applied to J/ψ legs or the two particle J/ψ system.

In addition to the J/ψ legs we require that the event should have a third track associated with the J/ψ vertex. The third track might be:

- the muon in the $B_c^+ \to J/\psi + \mu^+ + X$ decays, or
- the kaon in the $B^+ \to J/\psi + K^+$ sample, or
- a π^+, K^+ or p for the misidentified muon background calculation

Most requirements are the same as in the previous cross-section analysis [3], except the lifetime cut. In the previous analysis we applied a $ct > 60$ μm cut. However, based on the B_c^+ semileptonic lifetime analysis, we found that the $L_{xy}/\sigma_{L_{xy}} > 3$ is a better requirement to reduce the prompt J/ψ background. The cuts applied to the three track system are listed in Table II.

The invariant mass distribution of the $J/\psi + K^+$ is shown in Fig. 2. The B^+ sample size within our selection requirements is found to be 2333 ± 55 events. The combinatoric and possible $B^+ \to J/\psi + \pi^+$ contributions already are subtracted.

Using the selections for the three muon system, we collect 229 (214) $J/\psi + \mu^+$ candidate events within a $4 - 6$ GeV/c^2 signal mass window. In order to determine the number of B_c^+ signal events, we must calculate the background contributions to the sample and subtract them from the number of candidates.

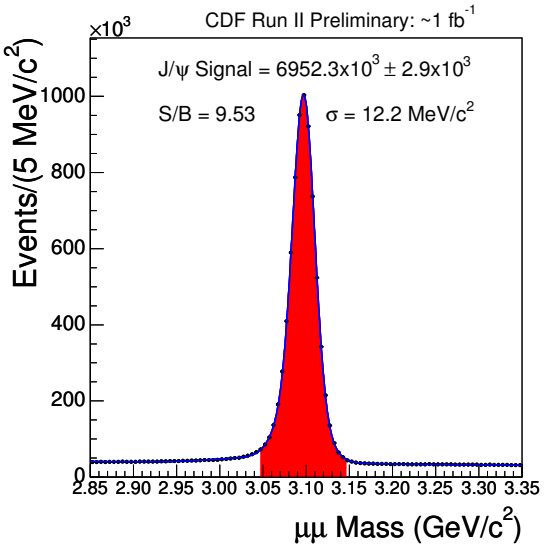

FIG. 1: Di-muon invariant mass distribution. The red region is the J/ψ signal mass window used for this analysis.

Selection requirement	Value	B_c^+	B^+	μ_{fake}
Muon Type	CMUP	X		
Muon Stub Matching	CMU χ^2(X Pos.)< 9.0	X		
CMUP Fiducial	Is Fiducial	X	X	X
Match with XFT	Is XFT	X	X	X
Isolation at CMU	No extrapolated track within 40 cm at CMU	X	X	X
p_T	> 3.0 GeV/c	X	X	X
COT Hits	2 Stereo + 2 Axial Superlayers (5 hits per SL)	X	X	X
dE/dx Hits	≥ 43 Hits	X	X	X
Silicon Hits	≥ 3 hits in ϕ layers (SVX+ISL)	X	X	X
Vertex Probability	> 0.001 (J/ψ mass unconstrained)	X	X	X
$\Delta\phi$	$< \pi/2$	X	X	X
$\sigma_{L_{xy}}$	< 200 μm	X	X	X
$L_{xy}/\sigma_{L_{xy}}$	> 3	X	X	X
B_c^+ Mass region	$\lvert M_{J/\psi+track} - 5.0$ GeV/$c^2\rvert < 1.0$ GeV/c^2	X		X
$J/\psi + K^+$ Mass Veto	$\lvert M_{J/\psi+K^+} - 5.279$ GeV/$c^2\rvert > 0.05$ GeV/c^2	X		X

TABLE II: Cuts applied to third track or the three particle $J/\psi + track$ system.

III. B_C^+ BACKGROUND

We consider the following background sources to the semileptonic B_c^+ decays:

- Misidentified J/ψ
- Misidentified third muon
- $b\bar{b}$ background
- Contributions from other decay modes (see Sec. IV)

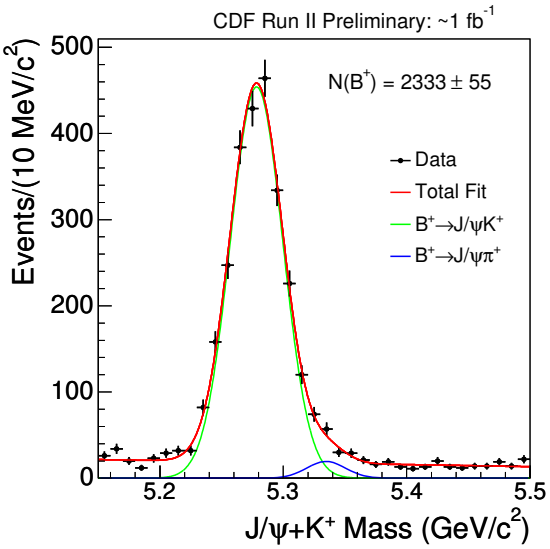

FIG. 2: The invariant mass distribution of the $J/\psi + K^+$ system from B^+ decays. The events passed the $p_T(J/\psi + K^+) > 4$ GeV/c cut.

A. Misidentified J/ψ background

The number of misidentified J/ψ plus real muons is estimated using the di-muons from the sidebands of the J/ψ mass. Our signal di-muon mass region is within ± 0.05 GeV/c^2 around the mean value of the measured J/ψ mass, $m_{J/\psi}$. The selected sideband regions are: $|m_{J/\psi} - 0.150 \text{ GeV}/c^2| < 0.05$ GeV/c^2 and $|m_{J/\psi} + 0.150 \text{ GeV}/c^2| < 0.05$ GeV/c^2.

Since the width of each sideband is the same as our signal region, we applied 1/2 weight for these events. We find 21.5 (20.5) events within the $4 - 6$ GeV/c^2 signal mass window. The events pass the $p_T(J/\psi_{side} + \mu^+) > 4$ GeV/c cut.

B. Misidentified muon background

The misidentified muon contribution to the B_c^+ background is calculated with the following steps:

- Determine the kaon and pion decay-in-flight and punch-through rates from a D^{*+} sample having the decay chain $D^{*+} \to D^0\pi^+$, $D^0 \to K^-\pi^+$ using the two track trigger datasets.
- Determine the pion, kaon, and proton fractions in the $J/\psi + track$ data using dE/dx and time-of-flight tools.
- Calculate the number of misidentified muons due to pion and kaon decay-in-flight and punch-through in the $B_c^+ \to J/\psi + \mu^+$ sample using the hadron fractions and the measured muon misidentification probabilities from the D^{*+}/D^0 sample.
- Estimate the number of misidentified muons due to punch-through from protons.

The misidentification probabilities derived from data assume that the π/K track, even after a possible kink in the $\pi(K) \to \mu + X$ decay-in-flight, will allow the reconstructed D^0 mass value to remain under the peak. The fraction of the events outside of the D^0 mass peak are accounted for with a special simulation study.

The proton probability to make a misidentified muon via the punch-through process is estimated using the proton tracks in $\Lambda \to p\pi$ decays. We are able to establish an upper limit for this process since it is so rare.

The π fraction F_π in the $J/\psi + track$ sample is determined using a dE/dx method. The K and p energy losses in the COT for our $p_T > 3$ GeV/c range are insufficient to separate them in the dE/dx distribution. Consequently, the K and p fractions F_{K+p} are combined. The proton fraction F_p is estimated within the $2 - 3$ GeV/c momentum region only using a simultaneous fit of the dE/dx and time-of-flight data. For higher momenta ($p > 3$ GeV/c) we follow the predictions for F_p from PYTHIA. Thus, the dE/dx returns the F_π and F_{K+p} fractions where F_p was fixed to values defined from data and Monte Carlo simulation.

The final muon misidentification probabilities (ϵ_π, ϵ_K and ϵ_p) and the particles fractions ($F_{\pi,K,p}$) in $J/\psi + track$ system are the same values used in the B_c^+ lifetime analysis [5]. In the lifetime analysis $F_{\pi,K,p}$ are calculated for 3 ct regions: $ct < 0$ μm, $0 < ct < 150$ μm and $ct > 150$ μm. In the B_c^+ to B^+ ratio analysis we use the fractions for positive ct values.

The three track system passes the minimum $p_T(J/\psi + track) > 4$ GeV/c cut. This sample is an input to calculate the misidentified muons. For each third track in this sample we assign a weight W,

$$W = \epsilon_\pi \cdot F_\pi + \epsilon_K \cdot F_K + \epsilon_p \cdot F_p, \tag{1}$$

where $\epsilon_{(\pi,K,p)}$ is the probability to misidentify a muon as a π, K, or p and F(π, K, p) is the fraction of a given particle within the $J/\psi + track$ sample. The weight W is applied on a track-by-track basis to calculate the weighted $J/\psi + track$ mass distribution.

Both the misidentified J/ψ and misidentified muon backgrounds have one common subsample: misidentified$_{J/\psi}$+misidentified$_\mu$. To avoid double counting, it is necessary to subtract it only once. To calculate the doubly misidentified background, we apply the same weighting procedure to the sideband J/ψ plus track sample using the misidentification probabilities and the π, K, and p fractions.

C. The $b\bar{b}$ background

We must also account for cases when the J/ψ is produced by a B hadron and the third muon is produced by a $\bar{B}$ hadron (or vice versa) in the same event. The basic procedure for the calculation is described in the semileptonic B_c^+ lifetime measurement [5]. Using the PYTHIA generator, we simulate the J/ψ production from one B ($\bar{B}$) hadron and force the other $\bar{B}$ (B) hadron in the same event to decay semileptonically via a muon. The B hadron decaying to the J/ψ includes the $J/\psi + K^+$ decay chain.

The number of $b\bar{b}$ events that pass the $J/\psi\mu$ selection cuts, $N_{b\bar{b}}$, is given by the formula

$$N_{b\bar{b}} = C_{norm}(S_{FC}N_{b\bar{b}}^{FC} + S_{FE}N_{b\bar{b}}^{FE} + S_{GS}N_{b\bar{b}}^{GS}) \times \frac{N_{B^+}^{data}}{S_{FC}N_{B^+}^{FC} + S_{FE}N_{B^+}^{FE} + S_{GS}N_{B^+}^{GS}}. \tag{2}$$

Here, $C_{norm} = 1.05 \pm 0.10$ is a parameter that accounts for the uncertainties in the simulation of J/ψ and muon production in B decays relative to the $B^+ \to J/\psi + K^+$ branching fraction and should be unity if the rates in the PYTHIA sample exactly match the physical values. The parameters S_{FC}, S_{FE}, and S_{GS} are the scale factors for the different QCD processes in PYTHIA that contribute to the $b\bar{b}$ background; $N_{b\bar{b}}^{FC}$, $N_{b\bar{b}}^{FE}$, and $N_{b\bar{b}}^{GS}$ are the number of PYTHIA generated events from the three QCD processes that pass the $J/\psi+\mu^+$ selection; N_{B^+} is the total number of $B^+ \to J/\psi+K^+$ decays in the data; and $N_{B^+}^{FC}$, $N_{B^+}^{FE}$, and $N_{B^+}^{GS}$ are the numbers of $B^+ \to J/\psi + K^+$ decays produced by the three QCD processes in PYTHIA. The last term is assigned for the normalization of the PYTHIA sample to data. The scale factors S_{FC}, S_{FE}, and S_{GS} are found by the fit of the ϕ distribution in the unvertexed $J/\psi+\mu^+$ sample. The scale factors are the same as used in the B_c^+ lifetime analysis: $S_{FE} = 0.83 \pm 0.34$, $S_{GS} = 1.42 \pm 0.21$ and $S_{FC} = 3 - S_{FE} - S_{GS}$ [5].

The final $b\bar{b}$ background contributions are summarized in Table III. The uncertainty in the $b\bar{b}$ background is due to several sources. There are statistical uncertainties in the six PYTHIA simulated samples: $N_{b\bar{b}}^{FC}$, $N_{b\bar{b}}^{FE}$, $N_{b\bar{b}}^{GS}$,$N_{B^+}^{FC}$, $N_{B^+}^{FE}$, and $N_{B^+}^{GS}$. There is the statistical uncertainty in the determination of the $B^+ \to J/\psi + K^+$ sample in the experimental data. Finally there are uncertainties in the parameters C_{norm}, S_{FC}, S_{FE}, and S_{GS} that are determined by the fit to the ϕ distribution in the unvertexed $J/\psi\mu$ sample plus additional correlations between all eleven of these quantities that are introduced by the fitting procedure. The final uncertainty for $N_{b\bar{b}}$ is less than the component uncertainties combined in quadrature because of the correlations among the various quantities used in the calculation of the $b\bar{b}$ background.

$b\bar{b}$ background	$N_{b\bar{b}}$(MC)	S_i	N_{B^+} (MC)	$N_{b\bar{b}}$ prediction
Flavor creation (FC)	0	$3 - S_{FE} - S_{GS}$	1534 ± 43	0
Flavor excitation (FE)	16	0.83 ± 0.34	3308 ± 60	5.8 ± 2.6
Gluon splitting (GS)	52	1.42 ± 0.21	1231 ± 36	31.9 ± 8.2
Total	68	-	-	37.7 ± 7.3

TABLE III: The predicted number of $b\bar{b}$ background events. The minimum $p_T(J/\psi + \mu^+) > 4$ GeV/c cut is applied. Uncertainties include statistical uncertainties due to the sample sizes of the simulated three muon systems, the number of simulated B^+, and uncertainties in the scale factors with their correlations determined from the fitting procedure.

D. Total background

The total background to the $B_c^+ \to J/\psi + \mu^+$ decays is summarized in Table IV. It includes the misidentified J/ψ, misidentified muon, and $b\bar{b}$ backgrounds. The doubly misidentified contribution is subtracted to avoid double counting.

B_c^+ backgrounds	$p_T(J/\psi + \mu^+) > 4$ GeV/c	$p_T(J/\psi + \mu^+) > 6$ GeV/c
Misidentified J/ψ	21.5 ± 3.3	20.5 ± 3.2
Misidentified muon	55.8 ± 2.0	53.6 ± 1.9
Doubly misidentified	-8.8 ± 0.4	-7.5 ± 0.3
$b\bar{b}$ background	37.7 ± 7.3	35.4 ± 7.0
Total background	106.2 ± 8.2	102.1 ± 8.0

TABLE IV: The total background for $B_c^+ \to J/\psi + \mu^+$ decays in the signal region $4 < m(J/\psi + \mu^+) < 6$ GeV/c^2. The doubly misidentified contribution is subtracted to avoid double counting. All uncertainties are statistical, except for the $b\bar{b}$ background, where the correlations and uncertainties in the QCD scale factors from the $\Delta\phi$ fitting procedure are included.

IV. CONTRIBUTIONS FROM OTHER DECAY MODES

After subtracting the backgrounds, the basic tri-muon sample that is reconstructed from data may still have contributions from other B_c^+ decay modes. For example, a B_c^+ might decay into $\psi(2S) + \mu^+ + \nu$ followed by $\psi(2S)$ decay into $J/\psi + ...$ Another example is a B_c^+ decay into $J/\psi + \tau^+ + \nu$ followed by the τ decay into a muon. The probability of events from these decays to survive our selection requirements is small, but non-zero.

In order to determine contributions from other decay modes, we generate 1×10^7 $B_c^+ \to J/\psi + \mu^+ + X$ decays associated with 11 other decay modes that may end-up in the tri-muon system. The

list of the considered decay modes and their surviving rates can be seen in Table V. The branching fractions of these decay modes are taken from theoretical predictions [6].

	B_c^+ decay mode	Rate relative to total decay rate
1	$J/\psi + \mu^+ + \nu$	0.9577
2	$J/\psi + \tau^+ + \nu$	0.0173
3	$\psi(2S) + \mu^+ + \nu$	0.0199
4	$\psi(2S) + \tau^+ + \nu$	0
5	$B_s^0 + \mu^+ + \nu$	0
6	$B_s^{*0} + \mu^+ + \nu$	0
7	$B^0 + \mu^+ + \nu$	0
8	$B^{*0} + \mu^+ + \nu$	0
9	$J/\psi + D_s^+$	0.0006
10	$J/\psi + D_s^{*+}$	0.0045
11	$J/\psi + D^+$	0
12	$J/\psi + D^{*+}$	0
	Total 3μ events	3118

TABLE V: The tri-muon survival rates from different decay modes that passed the B_c^+ selection requirements including the $p_T(3\mu) > 4$ GeV/c cut. The events were analyzed on the decay type based on the MC truth information.

V. THE B_C^+ EXCESS

The number of reconstructed $B_c^+ \to J/\psi + \mu^+ + \nu$ decay events after the background subtraction is summarized in Table VI. Using the number of B_c^+ events above the background, we are able to calculate the actual size of the contributions of the other decay modes. The contributions are: $0.133\times19.8 = 2.6\pm0.6$, $0.042\times122.8 = 5.2\pm0.5$ and $8.6\times0 = 0\pm0$ events for all three mass regions, respectively.

B_c^+ excess	$p_T(J/\psi + \mu^+) > 4$ GeV/c	$p_T(J/\psi + \mu^+) > 6$ GeV/c
$N(B_c^+ \to J/\psi + \mu^+ + X)$, observed	229 ± 15.1	214 ± 14.6
Total background	106.2 ± 8.2	102.1 ± 8.0
$N(B_c^+ \to J/\psi + \mu^+ + X)$, bg. sub.	122.8 ± 17.2	111.9 ± 16.6
Other decay modes	5.2 ± 0.5	4.8 ± 0.4
$N(B_c^+ \to J/\psi + \mu^+ + \nu)$, bg. sub.	117.6 ± 17.2	107.1 ± 16.7

TABLE VI: B_c^+ excess in the signal region $4 < m(J/\psi + \mu^+) < 6$ GeV/c^2. All uncertainties are statistical.

The invariant mass distribution of the $J/\psi + \mu^+$ candidate events is shown in Fig. 3 with Monte Carlo simulated signal and the backgrounds superimposed. "Misid. Muon" stands for the misidentified muon background with the doubly misidentified background subtracted, while "Other modes" indicates the contribution from the the other decay modes. "B_c Monte Carlo" stands for the simulated $B_c^+ \to J/\psi + \mu^+ + \nu$ decays. The simulated sample size is set to the number of signal events in the data after background subtraction. The chi-squared probability is calculated by grouping the data into bins of at least 20 events.

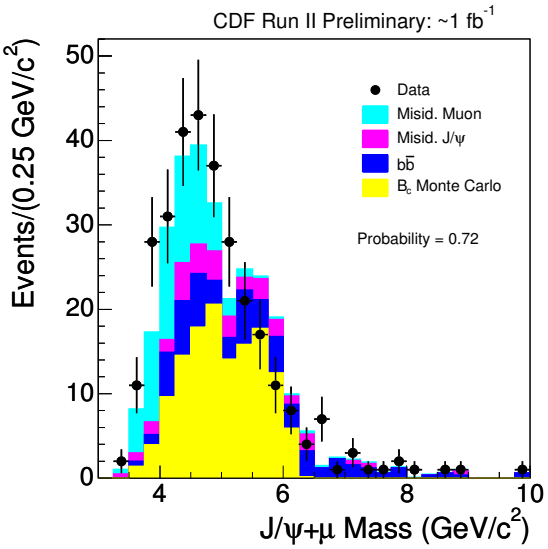

FIG. 3: The invariant mass distribution of the $B_c^+ \to J/\psi{+}\mu^+$ candidate events using 1 fb^{-1} data with Monte Carlo simulated sample and the backgrounds superimposed. The events passed the minimum $p_T(3\mu) > 4$ GeV/c cut. "Misid. Muon" stands for the misidentified muon minus the doubly misidentified background, while "Other modes" indicated the contribution from the other decay modes. "B_c Monte Carlo" stands for the simulated $B_c^+ \to J/\psi + \mu^+ + \nu$ decays. The chi-squared probability is calculated by grouping the data into bins of at least 20 events.

VI. RELATIVE EFFICIENCY

The ratio of the production cross section times branching ratio of the $B_c^+ \to J/\psi{+}\mu^+{+}\nu$ relative to the $B^+ \to J/\psi + K^+$ can be written as

$$\frac{\sigma(B_c^+) * BR(B_c^+ \to J/\psi + \mu^+ + \nu)}{\sigma(B^+) * BR(B^+ \to J/\psi + K^+)} = \frac{N_{B_c^+}}{N_{B^+}} \times \epsilon_{rel}, \tag{3}$$

where $N_{B_c^+}$ is finalized in Table VI within the signal mass region ($4-6$ GeV/c^2), the N_{B^+} is given in Fig. 2 and $\epsilon_{rel} = \epsilon_{B^+}/\epsilon_{B_c^+}$. We can determine the ϵ_{B^+} and $\epsilon_{B_c^+}$ by generating $B^+ \to J/\psi + K^+$ and $B_c^+ \to J/\psi{+}\mu^+{+}\nu$ decays, respectively. To generate the B^+ sample, we use the 2D $\eta - p_T$ spectrum based on CDF measurements [7]. As the input $\eta - p_T$ spectrum for the B_c^+, CDF previously used the theoretically-predicted distribution [8]. However, this spectrum is based on incomplete work, which was later updated and published [9]. In light of even more recent theoretical work on B_c^+ production, we decided to use the more complete B_c^+ spectrum from [10], which has the following advantages:

- It includes the B_c^{*+} as well as the B_c^+ spectra.
- The latest spectrum includes b and c quark contributions, as well as the pure g+g fusion mechanism.
- It includes a $q\bar{q}$ production contribution.

The left plot in Fig. 4 illustrates the differences between the previous B_c^+ spectrum used in CDF [11], which we refer to as the "Old B_c^+ spectrum" (black) and the updated spectrum, which we refer to as the "New B_c^+ GMVFN spectrum" (blue). The red histogram labeled "New B_c^+ FFN" illustrates the pure gluon-gluon fusion process. The right plot illustrates the B_c^+ and B_c^{*+} spectra based on the GMVFN model, black and blue plots, respectively. The red and green histograms illustrate the

$q + \bar{q}$ annihilation processes, which contributes very little to the overall spectrum as is seen in the next section (Sec VI A). One can see from the left plot that the "new" spectrum (blue graph) is softer than the "old" (black graph). The right plot illustrates that the B_c^+ and B_c^{*+} spectra are close to each other. However, the B_c^+ spectrum from the $B_c^{*+} \to B_c^+ + \gamma$ decays is softer that the direct B_c^+ production spectrum.

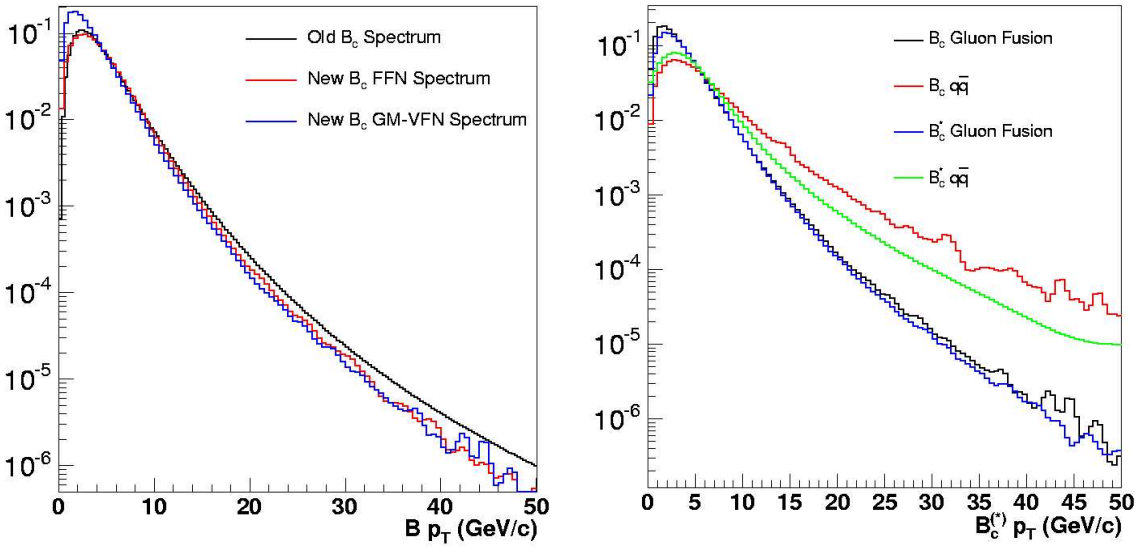

FIG. 4: The left plot illustrates the differences between has previously been used in CDF, called the "Old B_c^+ spectrum", and the updated spectrum based on the lated theoretical predictions [10], called the "New B_c^+ GMVFN spectrum". The red plot named as "New B_c^+ FFN" illustrates the pure gluon-gluon fusion process. The right plot illustrates the B_c^+ and B_c^{*+} spectra from the GMVFN model (black and blue) and from the quark-antiquark annihilation process (red and green).

A. B_c^+ spectrum

A new nominal spectrum selection based on the B_c^+ and B_c^{*+} cross sections is presented in Table I and II of reference [10]. According to this calculation, made for Tevatron energy $\sqrt{s} = 1.96$ GeV/c^2 using $p_T(B_c^+) > 4$ GeV/c and $|y| < 0.6$ cuts, the total production cross sections for the B_c^+ and B_c^{*+} are 0.7 nb and 2.3 nb, respectively. In Table VII we represent the same predictions in the form of the B_c^+ and B_c^{*+} production fractions relative to the total B_c^+ cross section. The first column represents the fractions of the combined contributions from g+g fusion, $g + \bar{b}$ and $g + c$ production subprocesses. The second column represents the fractions related to the quark-antiquark production mechanism. The third column represents the fractions of B_c^+ and B_c^{*+} cross sections relative to the combined total cross section.

Table VII suggests that the new nominal spectrum should be composed of 23.7% B_c^+ and 76.3% B_c^{*+}. The B_c^+ is produced 99.4% of the time from $gg + g\bar{b} + gc$ and in 0.6% from the $q+\bar{q}$ annihilation process. B_c^{*+} should be made in 99.1% of the time from gluon related mechanisms and 0.9% from the quark production process. The authors of [10] kindly supported us with the p_T and y distributions for both B_c^+ and B_c^{*+} mesons from the different production mechanisms.

For the B_c^{*+} mass we set $m(B_c^{*+}) = m(B_c^+) + 0.076$ GeV/c^2 based on the theoretically predicted value [12]. The systematic uncertainty due to the choice of B_c^{*+} mass is discussed in Sec. VII B 2. The B_c^{*+} lifetime is set to zero.

Production fractions	$gg + g\bar{b} + gc$	$q + \bar{q}$	Fractions of total σ
B_c^+	0.994	0.006	$\frac{\sigma(B_c^+)}{\sigma(B_c^+ + B_c^{*+})} = 0.237$
B_c^{*+}	0.991	0.009	$\frac{\sigma(B_c^{*+})}{\sigma(B_c^+ + B_c^{*+})} = 0.763$

TABLE VII: GMVFN model: B_c^+ and B_c^{*+} cross section fractions based on calculations from [10], where "$gg+g\bar{b}+gc$" represents the combined contributions from g+g fusion, $g+\bar{b}$ and $g+c$ production subprocesses, $q + \bar{q}$ represents the quark-antiquark production mechanism.

B. B^+ spectrum

The input p_T spectrum for B^+ Monte Carlo simulation is the experimentally measured spectrum for a b quark fragmenting to a B hadron as determined from inclusive J/ψ production [13]. Since this experimentally determined spectrum is slightly softer than the experimentally determined spectrum for B^+ measured in $B^+ \to J/\psi + K^+$ decays [7], we modify it accordingly. By using a set of weights we convert the original spectrum to the FONLL spectrum found in Ref. [14] which is in good agreement with the low p_T dependence of the spectrum determined from inclusive J/ψ production and and duplicates within experimental error the measured p_T dependence of the B^+ spectrum above 10 GeV/c.

C. Spectrum Comparison: Data vs Simulation

The p_T spectra for B_c^+ and B^+ compared with Monte Carlo simulation are shown in Fig. 5. Both plots are made with the requirement that the invariant mass value should be within the signal region. Both of the p_T data distributions shown in the figure have been background subtracted. Both the Monte Carlo generated curves and the data have been normalized to have equal areas. Both plots show good consistency between data and Monte Carlo simulation except for the $B^+ \to J/\psi + K^+$ distribution below 6 GeV/c. We assign a systematic error to account for discrepancies in the simulated and measured spectra.

D. $J/\psi\mu$ Mass Comparison: Data vs Monte Carlo

The invariant mass of the $J/\psi + \mu^+$ is presented in Fig. 6. This plot allow us to compare distributions from data and Monte Carlo simulation. The data plot is made with the background subtraction applied. The simulated sample is normalized to the data using the measured yield for the signal mass region. Figure 6 illustrates that Monte Carlo simulation is in reasonable agreement with the background subtracted data. In computing chi-squared probability the data are grouped into bins of at least 16 events.

E. Detector acceptance for $B^+ \to J/\psi + K^+$ decays

The B^+ acceptance is determined from Monte Carlo simulation. The signal events are not a subset of the generated events. Both sets of events are determined from a sample with a generator level requirement of $p_T(B^+) > 2.5$ GeV/c. The B^+ events which satisfy $p_T(B^+) > 4$ (6) GeV/c at generation are counted from this sample as the "generated" events, while the "signal" events are then passed through the detector and trigger simulation with all analysis cuts applied and a requirement that $p_T(J/\psi + K^+) > 4$ (6) GeV/c.

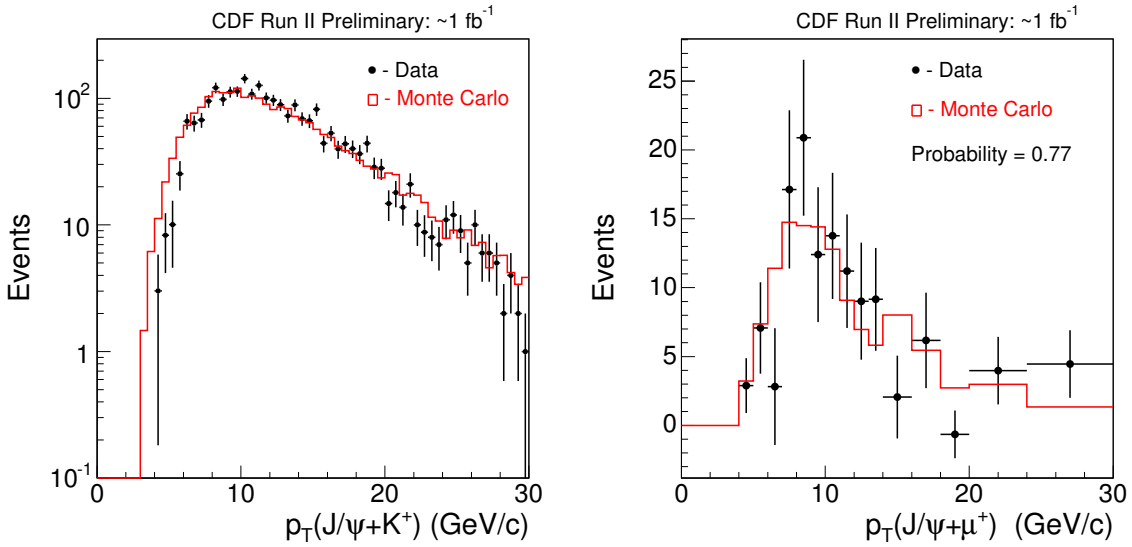

FIG. 5: The left plot illustrates the p_T spectra for $J/\psi + K^+$ and the right plot - for the $J/\psi + \mu$ samples. Both plot have been background subtracted. Both Monte Carlo spectra are scaled up to size of the data.

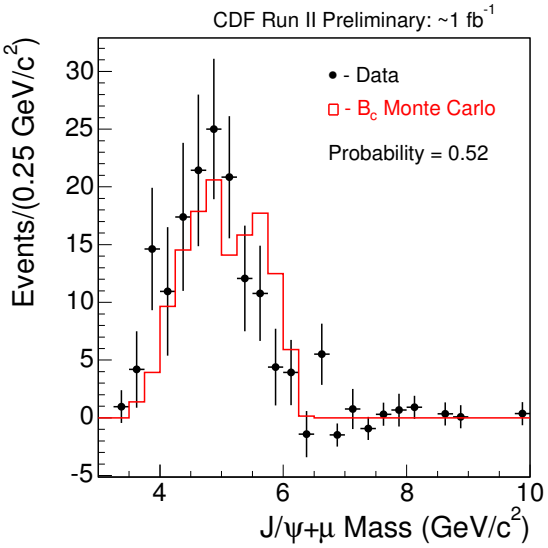

FIG. 6: The invariant mass of the $J/\psi + \mu^+$ system. The data plot is made with the background subtraction applied. The Monte Carlo sample is set to the same size as the data using the yield for the signal mass region. The chi-squared probability is calculated by grouping the data into bins of at least 16 events.

F. Detector acceptance for $B_c^+ \to J/\psi + \mu^+ + \nu$ decays

The calculation of the B_c^+ acceptance $\epsilon_{B_c^+}$ is analogous to the determination discussed in the previous section (Sec. VI E). The signal events are not a proper subset of the generated events. Both sets of events are determined from a sample with generator level requirement of $p_T(B_c^+) > 2.5$ GeV/c. The B_c^+ events which satisfy $p_T(B_c^+) > 4$ (6) GeV/c at generation are counted from this sample as the "generated" events, while the "signal" events are then passed through the detector and trigger

simulation with all analysis cuts applied and a requirement that $p_T(J/\psi+\mu^+) > 4$ (6) GeV/c. Consequently, detector smearing effects concerning the semileptonic B_c^+ decays are taken into account.

G. ϵ_{rel} results

The results for $\epsilon_{rel} = \epsilon_{B^+}/\epsilon_{B_c^+}$ with $p_T(B) > 4$ GeV/c and $p_T(B) > 6$ GeV/c cuts are presented in Table VIII.

Efficiencies	$p_T(B) > 4$ GeV/c	$p_T(B) > 6$ GeV/c
$\epsilon_{B_c^+}$ (%)	0.0551	0.1232
ϵ_{B^+} (%)	0.3231	0.6005
ϵ_{rel}	5.867 ± 0.068 (stat)	4.873 ± 0.060 (stat)

TABLE VIII: The relative efficiency ϵ_{rel} for $p_T(B) > 4$ GeV/c and $p_T(B) > 6$ GeV/c cuts.

VII. SYSTEMATIC UNCERTAINTIES

We divide the systematic uncertainties into two categories. The first represents the uncertainties on the number of B_c^+ signal events $N_{B_c^+}$. This covers the B_c^+ background systematics. The second represents the uncertainties in the relative efficiency. In this case we consider the ϵ_{rel} variations due to uncertainties in the knowledge of the B_c^+ lifetime and production spectrum, the B^+ production spectrum, and the relative efficiencies of kaons and muons due to triggering effects at the first level of the CDF II trigger (XFT).

A. B_c^+ background systematics

Below we discuss the following B_c^+ background systematics:

- Misidentified J/ψ
  - As this is derived from data, we do not assign a systematic uncertainty.
- Misidentified muon
  - We calculate the uncertainties by varying the proton fraction in the $J/\psi + track$ sample.
- $b\bar{b}$ background
  - We combine statistical and systematic uncertainties in the fit of the scale factors and their correlations. Consequently, no other systematic uncertainties are added to the estimate of the $b\bar{b}$ background.
- Other decay modes
  - We calculate the uncertainty by varying the branching ratios of the non-exclusive $B_c^+ \to J/\psi + \mu^+ + X$ decays.

Table IX summarizes all B_c^+ background systematics assigned. Details of individual systematics due to knowledge of the B_c^+ backgrounds are given in the following sections.

B_c^+ background systematics	$p_T(B) > 4$ GeV/c	$p_T(B) > 6$ GeV/c
Misidentified μ	5.7	5.5
Doubly misidentified	0.9	0.8
$b\bar{b}$	7.3 (st+sys)	7.0 (st+sys)
Other decay modes	$^{+6.0}_{-2.8}$	$^{+5.6}_{-2.5}$
Total	$^{+8.3}_{-6.4}$	$^{+7.9}_{-6.1}$

TABLE IX: Systematic uncertainties assigned for various backgrounds. The $b\bar{b}$ uncertainty was included in Table IV and is not included in the total systematic uncertainty given here.

1. Misidentified muon systematics

The largest source of uncertainties in the misidentified muon calculation is related to the proton fraction in the $J/\psi + track$ sample. The dE/dx method does not allow us to separate protons from kaons above 3 GeV/c. Consequently, we measure the proton fraction in the $2-3$ GeV/c momentum region using the ToF and dE/dx and then extrapolate the fraction to higher momenta according to PYTHIA predictions [5]. To estimate the systematic uncertainty, we consider the difference between the PYTHIA prediction and a flat proton fraction, as was done in the B_c^+ lifetime analysis.

2. Systematic uncertainty due to branching ratios

The systematic uncertainty due to poor knowledge of non-exclusive $B_c^+ \to J/\psi + \mu^+ + X$ branching ratios is estimated by varying of the branching ratios of 11 B_c^+ decay modes that may contribute to the tri-muon system. We consider two sets of branching ratio variations: twice and half of the nominal value with respect to the exclusive decay $B_c^+ \to J/\psi + \mu^+ + \nu$. The tri-muon rates from non-exclusive B_c^+ decay modes that pass all analysis cuts are shown in Table X. The rates are calculated for events which fall within the $4-6$ GeV/c^2 B_c^+ signal mass region.

	B_c^+ decay mode	Nominal	Double	Half
1	$J/\psi + \mu^+ + \nu$	0.9577	0.9131	0.9796
2	$J/\psi + \tau^+ + \nu$	0.0173	0.0354	0.0089
3	$\psi(2S) + \mu^+ + \nu$	0.0199	0.0387	0.0095
4	$\psi(2S) + \tau^+ + \nu$	0	0	0
5	$B_s^0 + \mu^+ + \nu$	0	0.0003	0
6	$B_s^{*0} + \mu^+ + \nu$	0	0	0
7	$B^0 + \mu^+ + \nu$	0	0	0
8	$B^{*0} + \mu^+ + \nu$	0	0	0
9	$J/\psi + D_s^+$	0.0006	0.0018	0.0003
10	$J/\psi + D_s^{*+}$	0.0045	0.0098	0.0016
11	$J/\psi + D^+$	0	0.0003	0
12	$J/\psi + D^{*+}$	0	0.0003	0
	Total 3μ events	3118	3280	3048

TABLE X: The tri-muons rates from different decay modes which pass the B_c^+ selection requirements, including the $p_T(3\mu) > 4$ GeV/c cut. The results are presented for the nominal, doubled and halved branching ratios.

B. Relative efficiency systematics

We consider following sources of uncertainty:

- B_c^+ lifetime
- B_c^+ production spectrum
- B^+ production spectrum
- K and μ differences in XFT simulation

The total ϵ_{rel} systematic uncertainty are summarized in Table XI. Details of the different systematic uncertainties are given in the following sections.

ϵ_{rel} systematics	$p_T(B) > 4$ GeV/c	$p_T(B) > 6$ GeV/c
B_c^+ lifetime	$^{+0.393}_{-0.223}$	$^{+0.354}_{-0.160}$
B_c^+ spectrum	0.720	0.298
B^+ spectrum	0.340	0.161
XFT trigger	0.192	0.160
Total	$^{+0.554}_{-0.450} \pm 0.720$ (spec.)	$^{+0.420}_{-0.278} \pm 0.298$ (spec.)

TABLE XI: ϵ_{rel} systematic uncertainties.

1. B_c^+ lifetime systematics

The B_c^+ lifetime systematic uncertainty is estimated by varying the B_c^+ lifetime within ± 14 μm relative to the default value. This variation represents one standard deviation of the current CDF result [5]. The default B_c^+ lifetime in the Monte Carlo simulation was set to 142.2 μm. To determine the systematic uncertainty, we generate two B_c^+ Monte Carlo samples with B_c^+ lifetimes of 128 μm and 156 μm.

2. B_c^+ production spectrum systematics

Theoretical predictions [8, 10] indicate that the b and c quark mass variations lead to small or negligible spectrum dependence. Consequently, we concentrated on the following variations:

- We double the $q\bar{q}$ contribution uncertainty based on predictions that suggest the uncertainty is at the level of the contribution itself [10].
- We evaluate the difference between the gluon fusion (FFN) model and the more complete $gg + g\bar{b} + gc$ (GMVFN) model.
- We estimate the difference between the combined $B_c^+ + B_c^{*+}$ and a purely B_c^+ spectrum. The prediction of the B_c^{*+} mass includes a range of masses based on different models [12]. We choose the largest mass difference between the B_c^{*+} and B_c^+ for the default result.

We assume that the variations we consider are independent and we add all variations in quadrature in order to obtain the total spectrum systematic uncertainty of 0.720 for $p_T(B_c^+) > 4$ GeV/c and 0.298 for $p_T(B_c^+) > 6$ GeV/c. These uncertainties are dominated by the difference in the FFN and GMVFN models.

3. B^+ production spectrum systematics

The left plot in Fig. 5 shows that above a p_T of 6 GeV/c the B^+ spectrum determined from the data is in reasonable agreement with the simulation, but that below 6 GeV/c the agreement is poor. It is suspected that this is due to the small experimental acceptance for the process $B^+ \to J/\psi K^+$ below 6 GeV/c. Figure 7 shows the p_T dependence of the B^+ acceptance. Below 6 GeV/c it is both small and falling very steeply. To estimate a systematic error in the relative efficiency we re-weight the simulated spectrum below 10 GeV/c to bring it into agreement with the data and recalculate the relative efficiency. We assign the difference between the previous value and the new value as a systematic uncertainty in the relative efficiency.

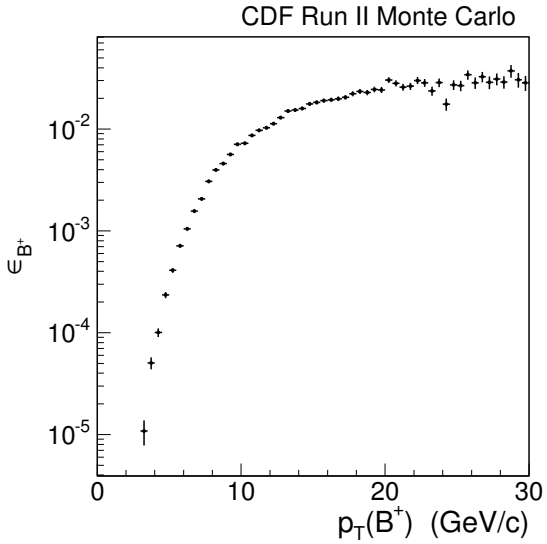

FIG. 7: Simulated B^+ acceptance as function of $p_T(B^+)$.

4. K and μ differences in XFT simulation

Another source of systematic uncertainty that we consider is the different XFT efficiencies of kaons and muons, which exist in the data, due to the number of hits required by the XFT in the drift chamber (COT), and which are not modeled in the simulation. We model this effect by re-weighting the transverse momentum of the kaon and muon according to the measured differences in the kaons and pions in data relative to Monte Carlo simulation [15], where we assume that the muon XFT efficiency is approximately equivalent to the pion XFT efficiency. Using the adjusted XFT efficiencies for kaons and pions affects the acceptance of both the B_c^+ and B^+.

VIII. CROSS SECTION RESULTS

Using B_c^+ and B^+ yields from Table VI and Fig. 2, respectively, and the ϵ_{rel} from Table VIII, we calculate the ratio of the production cross section time branching ratio of the $B_c^+ \to J/\psi + \mu^+ + \nu$ relative to the $B^+ \to J/\psi + K^+$. The final cross sections for the different p_T thresholds are presented in Table XII. Of the two results, the measurement for $p_T > 6$ GeV/c has the least systematic error. Below 6 GeV/c uncertainty in the B^+ acceptance appears to introduce a significant systematic discrepancy between the simulated spectrum and the spectrum as determined from the data. There

is also the possibility that the inclusive J/ψ spectrum is not a reliable way to determine the B^+ spectrum at low p_T.

Final results	$p_T(B) > 4$ GeV/c	$p_T(B) > 6$ GeV/c
$N(B_c^+ \to J/\psi + \mu^+ + \nu)$	117.6 ± 17.2 (stat) $^{+8.3}_{-6.4}$ (sys)	107.1 ± 16.7 (stat) $^{+7.9}_{-6.1}$ (sys)
$N(B^+ \to J/\psi + K^+)$	2333 ± 55 (stat)	2299 ± 53 (stat)
ϵ_{rel}	5.867 ± 0.068 (stat)	4.872 ± 0.060 (stat)
	$^{+0.554}_{-0.450}$ (sys) ± 0.720 (spectrum)	$^{+0.420}_{-0.278}$ (sys) ± 0.298 (spectrum)
$\frac{\sigma(B_c^+)*BR(B_c^+ \to J/\psi+\mu^+ +\nu)}{\sigma(B^+)*BR(B^+ \to J/\psi+K^+)}$	0.295 ± 0.040 (stat)	0.227 ± 0.033 (stat)
	$^{+0.033}_{-0.026}$ (sys) ± 0.036 (spectrum)	$^{+0.024}_{-0.017}$ (sys) ± 0.014 (spectrum)

TABLE XII: Results of B_c^+ production cross section times the branching ratio to $J/\psi + \mu^+ + \nu$ over B^+ production cross section times the branching ratio to $J/\psi + K^+$ are presented for two different p_T thresholds.

IX. CONCLUSION

We have performed a measurement of the relative production cross section of $B_c^+ \to J/\psi + \mu^+ + \nu$ in 1 fb^{-1} of exclusive J/ψ data. We have identified a sample of 229 (214) events with an estimated background from all sources of 111 ± 8 (107 ± 8) events for $p_T(B_c^+) > 4$ GeV/c (6 GeV/c).

For $p_T > 4$ GeV/c we obtain

$$\frac{\sigma(B_c^+) * BR(B_c^+ \to J/\psi + \mu^+ + \nu)}{\sigma(B^+) * BR(B^+ \to J/\psi + K^+)} = 0.295 \pm 0.040 \text{ (stat.)}^{+0.033}_{-0.026} \text{ (syst.)} \pm 0.036 \ (p_T \text{ spectrum}),$$

while for $p_T > 6$ GeV/c we find

$$\frac{\sigma(B_c^+) * BR(B_c^+ \to J/\psi + \mu^+ + \nu)}{\sigma(B^+) * BR(B^+ \to J/\psi + K^+)} = 0.227 \pm 0.033 \text{ (stat.)}^{+0.024}_{-0.017} \text{ (syst.)} \pm 0.014 \ (p_T \text{ spectrum}).$$

[1] Charge-conjugate states are implied throughout the paper unless otherwise specified.
[2] F. Abe et al. (CDF Collaboration), Phys. Rev. Lett. **81**, 2432 (1998); F. Abe et al. (CDF Collaboration), Phys. Rev. D **58**, 112004, (1998).
[3] http://www-cdf.fnal.gov/physics/new/bottom/050330.blessed-bc-jpsimu/.
[4] http://www-cdf.fnal.gov/physics/new/bottom/051029.blessed-BcJpsiE/.
[5] Mark Patrick Hartz, FERMILAB-THESIS-2008-82 (2008).
[6] M. A. Ivanov, J. G. Korner, and P. Santorelli, Phys. Rev. D **73**, 054024 (2006).
[7] A. Abulencia et al. (CDF Collaboration), Phys. Rev. D **75**, 012010 (2007).
[8] C.-H. Chang, C. Driouichi, P. Eerola, and X. G. Wu, Comput. Phys. Commun. **159**, 192 (2004), hep-ph/0309120.
[9] C.-H. Chang and X.-G. Wu, Eur. Phys. J. C **38**, 267 (2004).
[10] C.-H. Chang, C.-F. Qiao, J.-X. Wang, and X.-G. Wu, Phys. Rev. D **72**, 114009 (2005).
[11] A. Abulencia et al. (CDF Collaboration), Phys. Rev. Lett. **96**, 082002 (2006).
[12] M. Baldicchi and G. M. Prosperi, Phys. Rev. D **62**, 114024 (2000).
[13] D. E. Acosta et al. (CDF Collaboration), Phys. Rev. D **71**, 032001 (2005).
[14] M. Cacciari, S. Frixione, M. L. Mangano, P. Nason, and G. Ridolfi, JHEP **07**, 033 (2004).
[15] Karen Ruth Gibson, FERMILAB-THESIS-2006-09 (2006).